INTERNATIONAL JOURNAL FOR NUMERICAL METHODS IN FLUIDS
*Int. J. Numer. Meth. Fluids* (2009)
Published online in Wiley InterScience (www.interscience.wiley.com). DOI: 10.1002/fld.2190

# Unsteady MHD free convective heat and mass transfer from a vertical porous plate with Hall current, thermal radiation and chemical reaction effects

Ali Chamkha[1,*,†], M. A. Mansour[2] and Abdelraheem Aly[3]

[1]*Manufacturing Engineering Department, The Public Authority for Applied Education and Training, Shuweikh 70654, Kuwait*
[2]*Department of Mathematics, Faculty of Science, Assuit University, Assuit, Egypt*
[3]*Department of Mathematics, Faculty of Science, South Valley University, Qena, Egypt*

SUMMARY

An analysis is presented to investigate the effects of chemical reaction, thermal radiation and heat generation or absorption on unsteady free convective heat and mass transfer along an infinite vertical porous plate in the presence of a transverse magnetic field and Hall current. The governing partial differential equations are formulated and transformed by using a similarity transformation into a system of ordinary differential equations. The resulting equations are solved numerically using a fourth-order Runge–Kutta scheme along with the shooting method. The Rosseland approximation is used to describe the radiative heat flux in the energy equation. Numerical results for the velocity, temperature and concentration distributions are shown graphically for different parametric values. The effects of parameters on the local friction coefficients, the Nusselt number and Sherwood numbers are depicted in tabulated form. Copyright © 2009 John Wiley & Sons, Ltd.

Received 26 March 2009; Revised 18 June 2009; Accepted 17 August 2009

KEY WORDS: MHD; radiation; chemical reaction; unsteady flow; Hall current; heat generation/absorption

## 1. INTRODUCTION

In many transport processes existing in nature and in industrial applications in which heat and mass transfer is a consequence of buoyancy effects caused by diffusion of heat and chemical species. The study of such processes is useful for improving a number of chemical technologies, such as polymer production and food processing. In nature, the presence of pure air or water is impossible. Some foreign mass may be present either naturally or mixed with the air or water. Chemical reactions can be codified as either heterogeneous or homogeneous processes. This depends on whether they occur at an interface or as a single phase volume reaction. In well-mixed systems,

*Correspondence to: Ali Chamkha, Manufacturing Engineering Department, The Public Authority for Applied Education and Training, Shuweikh 70654, Kuwait.
†E-mail: achamkha@yahoo.com

Copyright © 2009 John Wiley & Sons, Ltd.

the reaction is heterogeneous, if it takes place at an interface and homogeneous, if it takes place in solution. In most cases of chemical reactions, the reaction rate depends on the concentration of the species itself.

In addition, in many fluid–particle flows, the fluid heat generation or absorption and the thermal radiation effects may play an important role in altering the heat transfer characteristics. Fan *et al.* [1] studied the mixed convective heat and mass transfer over a horizontal moving plate with a chemical reaction effect. Hossain and Ahmed [2] studied the combined effects of forced and free convection with uniform surface heat flux conditions in the presence of a strong magnetic field. Chamkha and Khaled [3] investigated the problem of coupled heat and mass transfer by magnetohydrodynamics (MHD) free convection from an inclined plate in the presence of internal heat generation or absorption. Vajravelu and Nayfeh [4] and Vajravelu and Hadjinicolaou [5] have considered the effects of temperature-dependent heat generation or absorption on heat transfer in different geometries. Anjali Devi and Kandasamy [6] have studied the effects of chemical reaction, heat and mass transfer on non-linear MHD laminar boundary-layer flow over a wedge with suction or injection. Sieniutycz [7] has studied non-linear macro-kinetics of heat and mass transfer and chemical or electrochemical reactions. Thermal radiation effects in particulate suspensions are especially important in multiphase systems consisting of solid particulates and gases. Thermal radiation within these systems is usually the result of emission by the hot walls and the gas–particle mixture. This radiation undergoes complex interaction with the system, primary due to absorption and scattering processes.

There has been a renewed interest in studying MHD flow and heat transfer in porous and non-porous media due to the effect of magnetic fields on the boundary layer flow control and on the performance of many systems using electrically conducting fluids. In addition, this type of flow has attracted the interest of many investigators in view of its applications in many engineering problems such as MHD generators, plasma studies, nuclear reactors, geothermal energy extractions. The unsteady hydromagnetic free convective flow with Hall current is studied by Singh and Raptis [8]. Ram [9] studied the effects of Hall and ion-slip currents on free convective heat-generating flow in a rotating fluid. Seddeek and Abeldahab [10] studied the Radiation effects on Unsteady MHD free convection with the Hall current near an infinite vertical porous plate. Sattar and Hossain [11] studied the effects of Hall current and mass transfer on unsteady hydromagnetic free convection flow along an accelerated porous plate with time-dependent temperature and concentration. In that paper Sattar and Hossain [11] introduced a similarity parameter (taken as a function of time) in order to make the governing equations locally similar. Moreover, Sattar, Alam and coworkers [12–16] employed similarity transformations for the study of Hall current and mass transfer on unsteady hydromagnetic free convection flow in different geometries.

The objective of the present work is to study the effects of Hall current, heat generation or absorption, thermal radiation and chemical reaction on unsteady MHD free convection near an infinite vertical porous plate. Similarity transformations are used to transform the governing partial differential equations to ordinary differential equations which are then solved numerically using the fourth-order Runge–Kutta integration scheme.

## 2. MATHEMATICAL ANALYSIS

Consider unsteady free convection flow of a viscous incompressible and electrically conducting fluid, along an infinite vertical porous plate subjected to time-dependent suction velocity. The flow

Copyright © 2009 John Wiley & Sons, Ltd.

DOI: 10.1002/fld

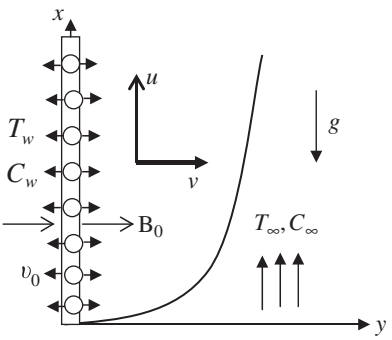


Figure 1. Physical configuration and coordinates system.

is assumed to be in the $x$-direction, which is taken along the plate in the upward direction and the $y$-axis perpendicular to it (see Figure 1). Uniform strong magnetic field $B_0$ is assumed to be applied in the $y$-direction. The fluid properties are assumed to be constant and a first-order homogeneous chemical reaction is assumed to take place in the flow. Under these assumptions with the usual Boussinesq approximation, the governing boundary-layer equations that are based on the balance laws of mass, linear momentum, energy and concentration species for this investigation can be written as

$$\frac{\partial \upsilon}{\partial y}=0 \tag{1}$$

$$\frac{\partial u}{\partial t}+\upsilon\frac{\partial u}{\partial y}=g\beta_T(T-T_\infty)+g\beta_C(C-C_\infty)+\nu\frac{\partial^2 u}{\partial y^2}-\frac{\sigma\mu_e^2B_0^2}{\rho(1+m^2)}(u+mw) \tag{2}$$

$$\frac{\partial w}{\partial t}+\upsilon\frac{\partial w}{\partial y}=\nu\frac{\partial^2 w}{\partial y^2}+\frac{\sigma\mu_e^2B_0^2}{\rho(1+m^2)}(mu-w) \tag{3}$$

$$\frac{\partial T}{\partial t}+\upsilon\frac{\partial T}{\partial y}=\frac{k}{\rho C_P}\frac{\partial^2 T}{\partial y^2}-\frac{1}{\rho C_P}\frac{\partial q_r}{\partial y}+\frac{Q_0}{\rho C_P}(T-T_\infty) \tag{4}$$

$$\frac{\partial C}{\partial t}+\upsilon\frac{\partial C}{\partial y}=D\frac{\partial^2 C}{\partial y^2}-k_c(C-C_\infty) \tag{5}$$

where $(u, w)$ are the $x$ and $z$ components of velocity, $\upsilon$ is the suction velocity, $T$ and $C$ are the temperature and concentration of the fluid, $\nu$ is the kinematics viscosity, $\sigma$ is the electric conductivity, $B_0$ is the strength of magnetic field, $\rho$ is the density, $q_r$ is the radiative heat flux. $k_c$ is the rate of chemical reaction, $g$ is the acceleration due to gravity, $\beta_T$ is the volumetric coefficient of thermal expansion, $\beta_C$ is the volumetric coefficient of concentration expansion. $D$ is the coefficient of mass diffusivity. $Q_0$ is heat generation or absorption constant. $T_\infty$ and $C_\infty$ are the free stream temperature and concentration, respectively. $\mu_e$ and $m$ are the magnetic permeability and Hall parameter, respectively.

Copyright © 2009 John Wiley & Sons, Ltd.

DOI: 10.1002/fld

The radiative heat flux term is simplified by using the Rosseland approximation (see Sparrow and Cess [17]) as

$$q_r = -\frac{4\sigma_0}{3k^*}\frac{\partial T^4}{\partial y} \tag{6}$$

where $\sigma_0$ and $k^*$ are the Stefan–Boltzman constant and the mean absorption coefficient, respectively. The obtained Taylor series expansion for $T^4$ neglecting higher-order terms:

$$T^4 = 4T_\infty^3 T - 3T_\infty^4 \tag{7}$$

Using Equations (6) and (7) in energy equation (4) we obtain

$$\frac{\partial T}{\partial t} + \upsilon\frac{\partial T}{\partial y} = \frac{v}{Pr}\left(1+\frac{4}{3R}\right)\frac{\partial^2 T}{\partial y^2} + \frac{Q_0}{\rho C_P}(T - T_\infty) \tag{8}$$

where $Pr = \rho v C_P/k$ is the Prandtl number and $R = kk^*/4\sigma T_\infty^3$ is the radiation parameter.

The boundary conditions are given by

$$\begin{aligned} &u = 0, \quad \upsilon = \upsilon_0(t), \quad w = 0, \quad T = T_w \quad \text{and} \quad C = C_w \quad \text{at } y = 0 \\ &u \to 0, \quad w \to 0, \quad T \to T_\infty \quad \text{and} \quad C \to C_\infty \quad \text{at } y \to \infty \end{aligned} \tag{9}$$

where $T_w$ and $C_w$ are the constant wall temperature and concentration, respectively. $\upsilon_0(t)$ is the time-dependent suction/ injection velocity at the porous plate.

The similar transformations are as follows:

$$u = u_0 f(\eta), \quad w = u_0 G(\eta), \quad \theta(\eta) = \frac{T - T_\infty}{T_w - T_\infty}, \quad \phi(\eta) = \frac{C - C_\infty}{C_w - C_\infty}, \quad \eta = \frac{y}{h} \tag{10}$$

where $h(=h(t))$ is a similarity parameter length scale and $u_0$ is free stream velocity. In terms of $h(t)$, a convenient solution of (1) can be given by

$$\upsilon = -\upsilon_0\left(\frac{u}{h}\right) \tag{11}$$

where $\upsilon_0$ is a non-dimensional transpiration parameter.

Substituting Equations (10) and (11) into Equations (2), (3), (5) and (8) yields

$$-\frac{h}{v}\frac{\mathrm{d}h}{\mathrm{d}t}\eta f' - \upsilon_0 f' = f'' + Gr\theta + Gc\phi - \frac{M}{(1+m^2)}(f + mG) \tag{12}$$

$$-\frac{h}{v}\frac{\mathrm{d}h}{\mathrm{d}t}\eta G' - \upsilon_0 G' = G'' + \frac{M}{(1+m^2)}(mf - G) \tag{13}$$

$$-\frac{h}{v}\frac{\mathrm{d}h}{\mathrm{d}t}\eta\theta' - \upsilon_0\theta' = \frac{1}{Pr}\left(1+\frac{4}{3R}\right)\theta'' + Q\theta \tag{14}$$

$$-\frac{h}{v}\frac{\mathrm{d}h}{\mathrm{d}t}\eta\phi' - \upsilon_0\phi' = \frac{1}{Sc}\phi'' - \gamma\phi \tag{15}$$

where $Gr = g\beta_T h^2(T_w - T_\infty)/vu_0$ is the local Grashof number, $Gc = g\beta_C h^2(C_w - C_\infty)/vu_0$ is the local modified Grashof number, $M = \sigma\mu_e^2 B_0^2 h^2/\rho v$ is the square of the Hartmann number or the

Copyright © 2009 John Wiley & Sons, Ltd.

DOI: 10.1002/fld

magnetic field, $Q=Q_0h^2/\rho\nu C_P$ is the heat generation or absorption parameter, $\gamma=k_ch^2/\nu$ is the chemical reaction parameter and $Sc=\nu/D$ is the Schmidt number.

To obtain similarity equations, assume that

$$\left(\frac{h}{\nu}\right)\frac{\mathrm{d}h}{\mathrm{d}t}=C^* \tag{16}$$

where $C^*$ is the arbitrary constant. By taking $C^*=2$ and integrating Equation (16) one obtains $h=2\sqrt{\nu t}$ which establishes the scaling parameter for unsteady boundary layer problems [10, 18].

Introducing Equations (16) with $C^*=2$ into Equations (12)–(15), we obtain the following dimensionless non-linear ordinary differential equations which are locally similar in time but not explicitly time dependent:

$$f''+2(\eta+a_0)f'+Gr\theta+Gc\phi-\frac{M}{(1+m^2)}(f+mG)=0 \tag{17}$$

$$G''+2(\eta+a_0)G'+\frac{M}{(1+m^2)}(mf-G)=0 \tag{18}$$

$$\frac{1}{Pr}\left(1+\frac{4}{3R}\right)\theta''+Q\theta+2(\eta+a_0)\theta'=0 \tag{19}$$

$$\frac{1}{Sc}\phi''-\gamma\phi+2(\eta+a_0)\phi'=0 \tag{20}$$

where $a_0=\upsilon_0/2$.

The non-dimensional boundary conditions can be written as:

$$\begin{aligned} &f=0, \quad G=0, \quad \theta=1, \quad \phi=1 \quad \text{at } \eta=0\\ &f\to 0, \quad G\to 0, \quad \theta\to 0, \quad \phi\to 0, \quad \eta\to\infty \end{aligned} \tag{21}$$

Of special significance for this type of flow and heat and mass transfer situation are the skin-friction coefficient, the Nusselt number $Nu$ and the Sherwood number $Sh$. The wall shear stresses in the $x$-direction and $z$-direction $\tau_x$, $\tau_z$, the surface heat flux, $q_\mathrm{w}$ and the surface mass flux $m_\mathrm{w}$ are defined as:

$$\tau_x=\mu\left.\frac{\partial u}{\partial y}\right|_{y=0}=\frac{\mu u_0}{h}f'(0), \quad \tau_z=\mu\left.\frac{\partial w}{\partial y}\right|_{y=0}=\frac{\mu u_0}{h}G'(0) \tag{22}$$

$$q_\mathrm{w}=-k\left.\frac{\partial T}{\partial y}\right|_{y=0}-\frac{4\sigma_0}{3k^*}\left(\frac{\partial T^4}{\partial y}\right)_{y=0}=[-\theta'(0)](T_\mathrm{w}-T_\infty)\frac{k}{h}\left(1+\frac{4}{3R}\right) \tag{23}$$

$$m_\mathrm{w}=-D\left.\frac{\partial C}{\partial y}\right|_{y=0}=[-\phi'(0)](C_\mathrm{w}-C_\infty)\frac{D}{h} \tag{24}$$

Then the skin-friction coefficients in the $x$-direction and $z$-direction, the local Nusselt number and the local Sherwood number are, respectively, given by

$$C_x=\frac{2\tau_x}{\rho u_0^2}=2Re^{-1}f'(0), \quad C_z=\frac{2\tau_z}{\rho u_0^2}=2Re^{-1}G'(0) \tag{25}$$

Copyright © 2009 John Wiley & Sons, Ltd.

DOI: 10.1002/fld

$$Nu = \frac{q_w}{(T_w - T_\infty)}\left(\frac{h}{k}\right) = -\left(1 + \frac{4}{3R}\right)\theta'(0) \tag{26}$$

$$Sh = \frac{m_w}{(C_w - C_\infty)}\left(\frac{h}{D}\right) = -\phi'(0) \tag{27}$$

where $Re = u_0 h/v$ is the Reynolds number.

## 3. NUMERICAL METHOD

The governing equations (17)–(20) subject to the boundary conditions (21) are solved numerically using the fourth-order Runge–Kutta integration scheme. The numerical procedure used here solves the two-point boundary value problems for a system of $N$ ordinary differential equations in the range $(x, x_1)$. The system of equations is written in the form

$$\frac{dy_i}{dx} = f_i(x, y_1, y_2, \ldots, y_N), \quad i = 1, 2, \ldots, N \tag{28}$$

and the equations are evaluated by a procedure that evaluates the derivatives of $y_1, y_2, \ldots, y_N$ at a general point $x$. Initially, $N$ boundary values of the variable $y_i$ must be specified, some of which will be specified at $x$ and some at $x_1$. The remaining $N$ boundary values are guessed and the procedure corrects them by a form of Newtonian iteration. Starting from the known and guessed values of $y_i$ at $x$, the procedure integrates the equations forward to a matching point $R$ using Merson's method. Similarly, starting from $x_1$ it integrates backwards to $R$. The difference between the forward and backward values of $y_i$ at $R$ should be zero for a true solution. The procedure uses a generalized Newton method to reduce these differences to zero, by calculating corrections to the estimated boundary values. This process is repeated iteratively until the convergence is obtained to a specified accuracy. The tests for convergence and the perturbation of the boundary conditions are carried out in a mixed form, for example, if the error estimate for $y_i$ is $\mathrm{ERROR}_i$, we test whether $\mathrm{ABS}(\mathrm{ERROR}_i) < \mathrm{ERROR}_i \times [1 + \mathrm{ABS}(y_i)]$.

In the present problem, a solution was considered to be converged if the newly calculated values of $f$, $G$, $\theta$ and $\varphi$ differed from their previous guessed values within a tolerance $E < 10^{-5}$. The numerical results were found to be dependent on $\eta_\infty$ and the step size. We have used $\Delta\eta = 0.01$ and $\eta_\infty = 4$ without causing numerical oscillations in the values $f$, $f'$, $G$, $G'$, $\theta$, $\theta'$, $\phi$ and $\varphi'$.

## 4. RESULTS AND DISCUSSION

In order to get a clear insight of the physical problem, numerical results are displayed with the help of graphical illustrations. The system of equations (17)–(20) with the boundary conditions (21) was solved numerically by the Runge–Kutta integration scheme. Computations were carried out for the various values of physical parameters such as the chemical reaction parameter $\gamma$, magnetic field parameter $M$, Hall parameter $m$, heat generation or absorption parameter $Q$, radiation parameter $R$, Prandtl number $Pr$ and the Schmidt number $Sc$. Figures 2–16 illustrate the influence of the material parameters on the velocity, temperature and the concentration profiles while Tables I–III summarize the effects of these parameters on the values of the skin-friction coefficients, the Nusselt number and the Sherwood number.

Copyright © 2009 John Wiley & Sons, Ltd.

DOI: 10.1002/fld

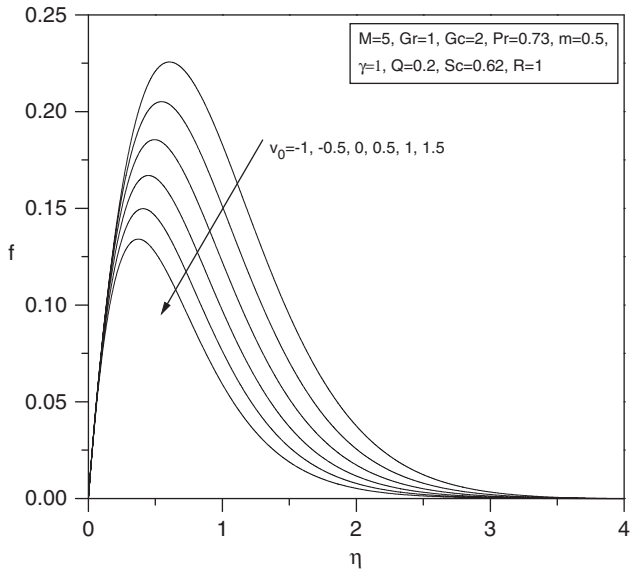


Figure 2. Effects of the suction/injection parameter on the primary velocity profiles.

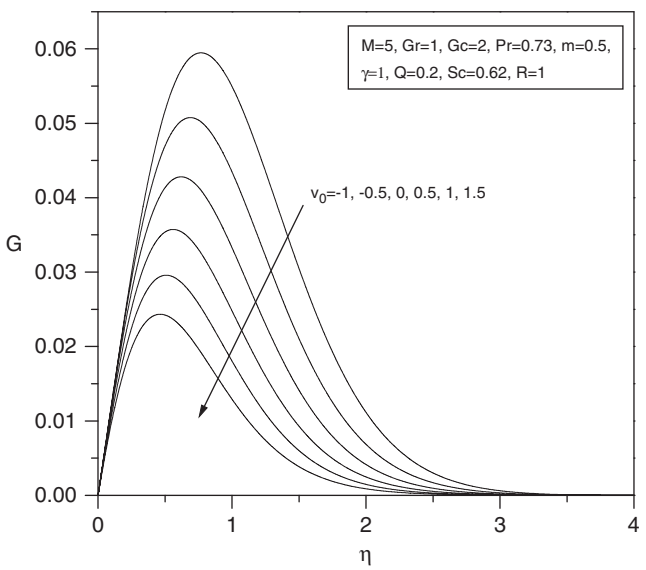


Figure 3. Effects of the suction/injection parameter on the secondary velocity profiles.

Copyright © 2009 John Wiley & Sons, Ltd.

DOI: 10.1002/fld

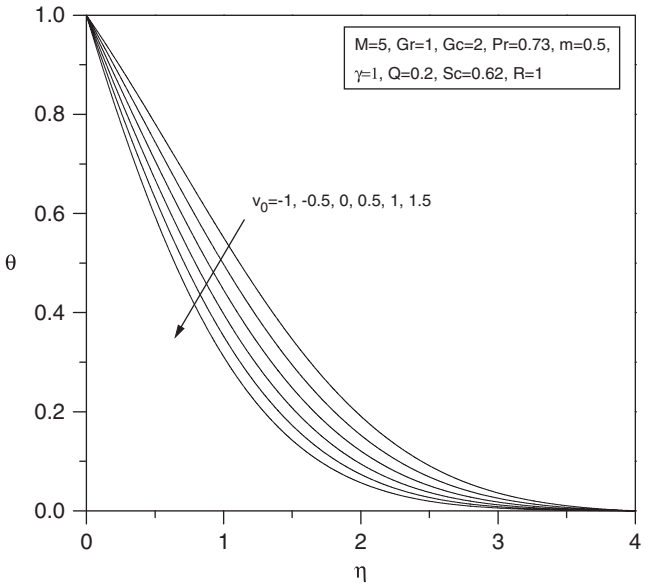


Figure 4. Effects of the suction/injection parameter on the temperature profiles.

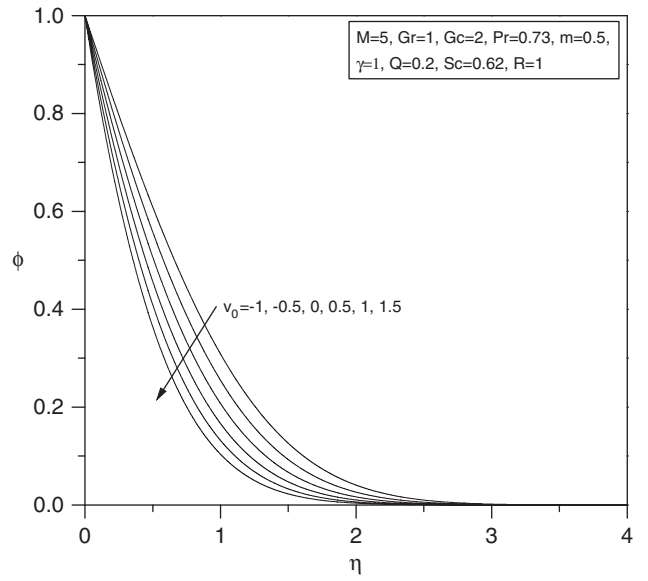


Figure 5. Effects of the suction/injection parameter on the concentration profiles.

Copyright © 2009 John Wiley & Sons, Ltd.

DOI: 10.1002/fld

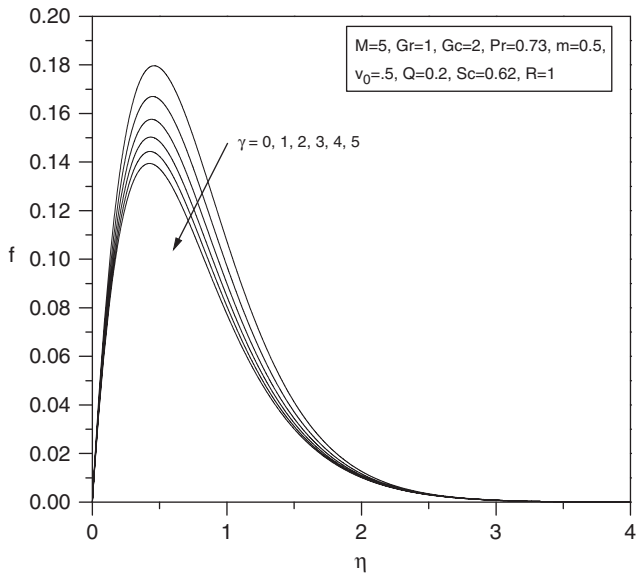


Figure 6. Effects of the chemical reaction parameter on the primary velocity profiles.

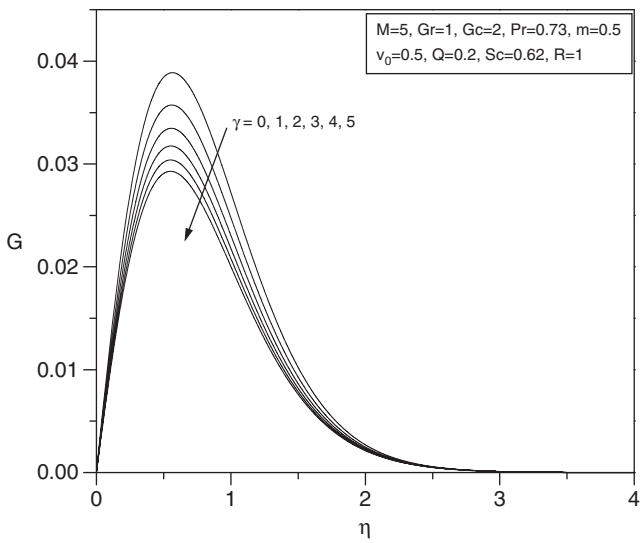


Figure 7. Effects of the chemical reaction parameter on the secondary velocity profiles.

Copyright © 2009 John Wiley & Sons, Ltd.

DOI: 10.1002/fld

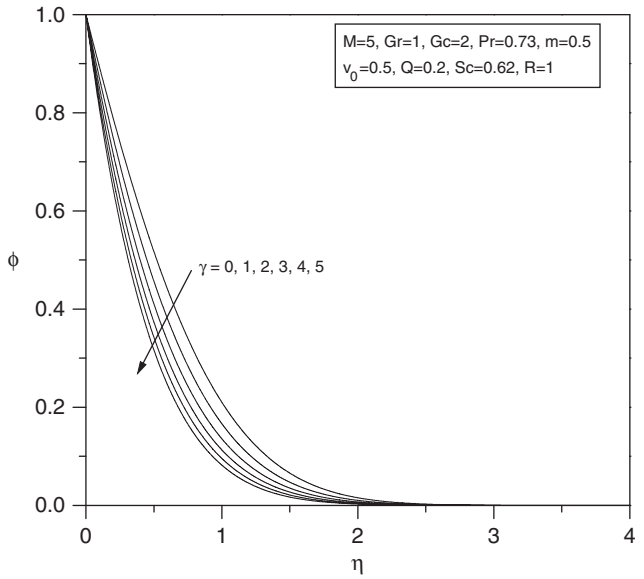


Figure 8. Effects of the chemical reaction parameter on the concentration profiles.

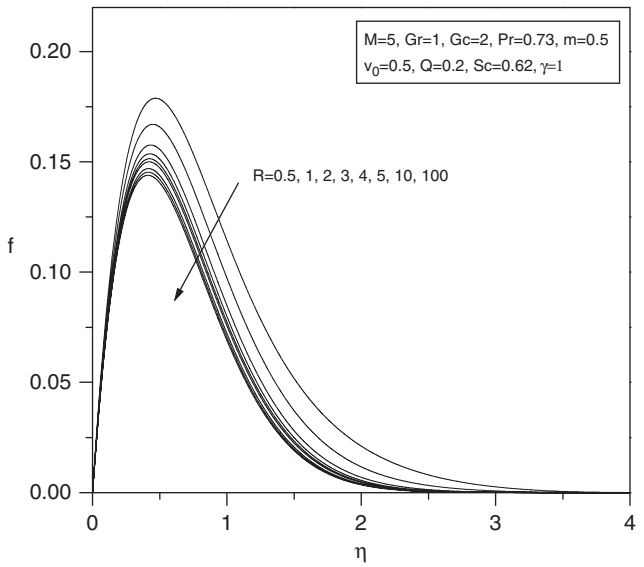


Figure 9. Effects of the radiation parameter on the primary velocity profiles.

Copyright © 2009 John Wiley & Sons, Ltd.

DOI: 10.1002/fld

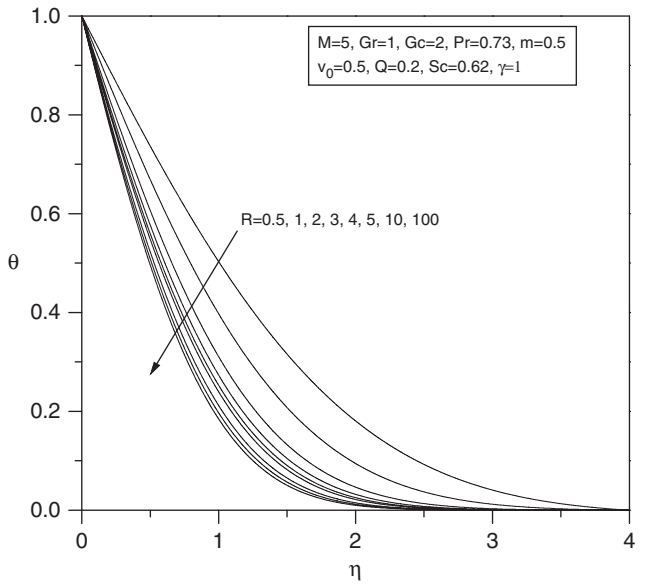


Figure 10. Effects of the radiation parameter on the temperature profiles.

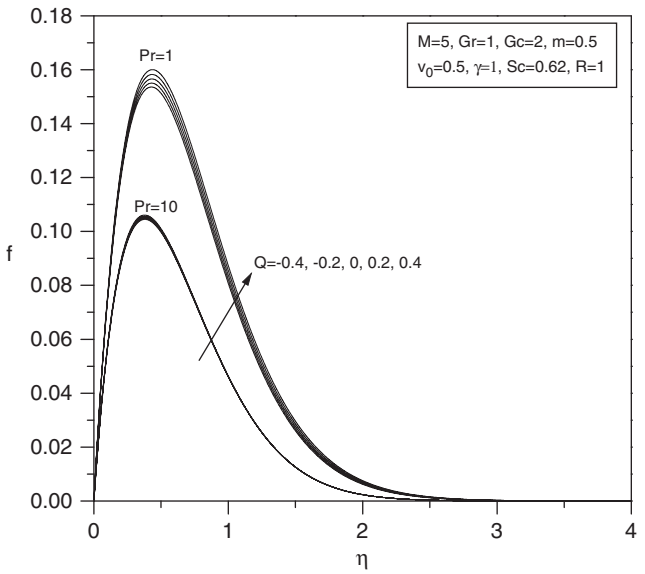


Figure 11. Effects of the heat generation/absorption parameter on the primary velocity profiles.

Copyright © 2009 John Wiley & Sons, Ltd.

DOI: 10.1002/fld

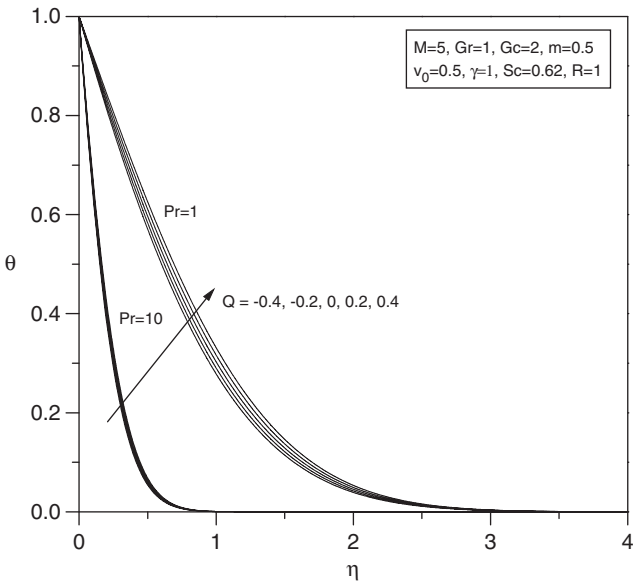


Figure 12. Effects of the heat generation/absorption parameter on the temperature profiles.

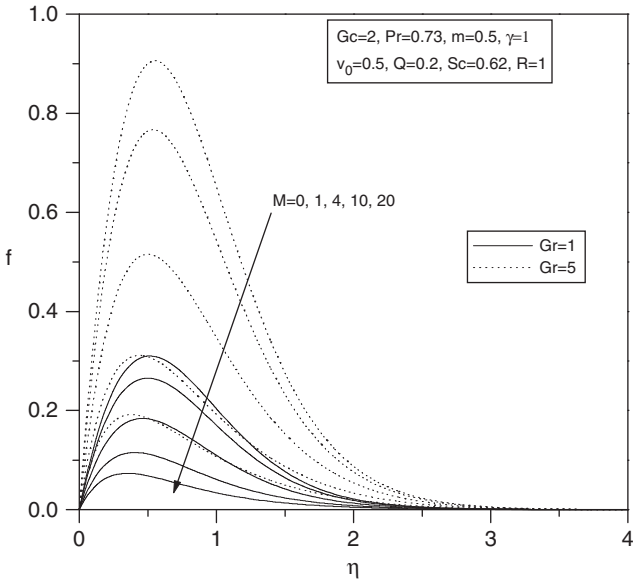


Figure 13. Effects of the magnetic field parameter on the primary velocity profiles.

Copyright © 2009 John Wiley & Sons, Ltd.

DOI: 10.1002/fld

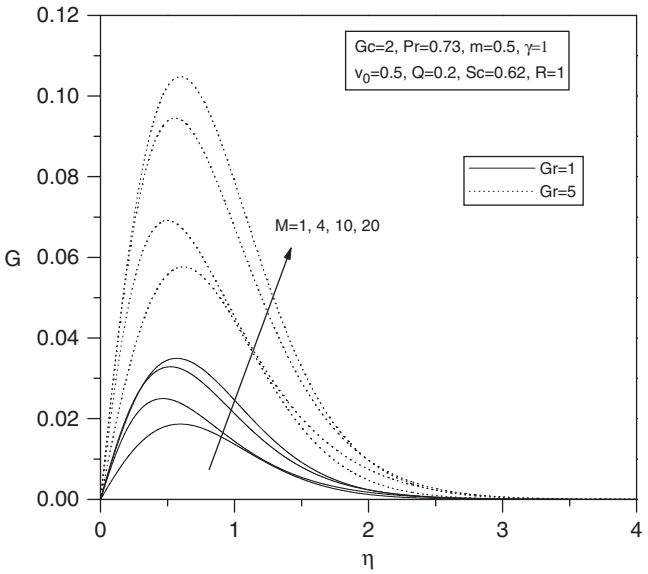


Figure 14. Effects of the magnetic field parameter on the secondary velocity profiles.

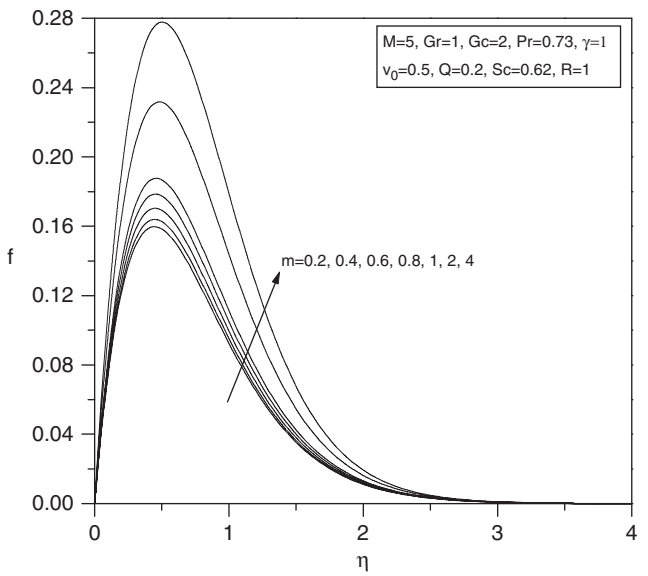


Figure 15. Effects of the Hall parameter on the primary velocity profiles.

Copyright © 2009 John Wiley & Sons, Ltd.

DOI: 10.1002/fld

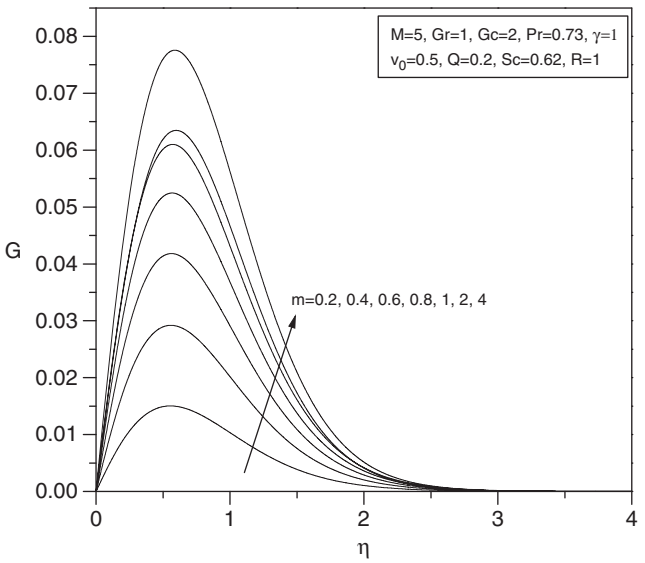


Figure 16. Effects of the Hall parameter on the secondary velocity profiles.

Table I. Values of $f'(0)$, $G'(0)$ and $-\theta'(0)$ for various values of $Gr$, $Pr$ and $M$ for $Gc=2$, $Q=0.2$, $Sc=0.62$, $R=1$, $\upsilon_0=0.5$, $\gamma=1$ and $m=0.5$.

| $Gr$ | $Pr$ | $M$ | $f'(0)$ | $G'(0)$ | $-\theta'(0)$ |
|---|---|---|---|---|---|
| 0 | 0.3 | 5 | 0.568575 | 0.06508 | 0.436954 |
| | 1 | | 0.568575 | 0.06508 | 0.830676 |
| | 10 | | 0.568575 | 0.06508 | 3.711416 |
| 5 | 0.3 | | 2.667677 | 0.446024 | 0.436954 |
| | 1 | | 2.26936 | 0.300199 | 0.830676 |
| | 10 | | 1.319748 | 0.107256 | 3.711416 |
| 10 | 0.3 | | 4.766779 | 0.826969 | 0.436954 |
| | 1 | | 3.970146 | 0.535319 | 0.830676 |
| | 10 | | 2.070921 | 0.149433 | 3.711416 |
| 1 | 0.73 | 0.1 | 1.380519 | 0.007598 | 0.691974 |
| | | 1 | 1.257009 | 0.057871 | 0.691974 |
| | | 5 | 0.9331 | 0.120081 | 0.691974 |
| | | 10 | 0.745692 | 0.121217 | 0.691974 |

Figures 2–5 present typical primary velocity $f$, secondary velocity $G$, temperature and concentration profiles in the boundary layer for various values of the non-dimensional transpiration parameter $\upsilon_0$, respectively. These figures show that the primary velocity, secondary velocity, temperature and concentration profiles are higher for injection conditions ($\upsilon_0<0$) compared with suction conditions ($\upsilon_0>0$). In addition, it can be seen that for cooling of the plate ($Gr>0, Gc>0$), the velocity profiles decrease monotonically with the increase of the suction parameter indicating

Copyright © 2009 John Wiley & Sons, Ltd.

DOI: 10.1002/fld

Table II. Values of $f'(0)$, $G'(0)$ and $-\phi'(0)$ for various values of $Gc$, $Sc$ and $m$ for $Gr=1$, $Q=0.2$, $Pr=0.73$, $R=1$, $\upsilon_0=0.5$, $\gamma=1$ and $M=5$.

| $Gc$ | $Sc$ | $m$ | $f'(0)$ | $G'(0)$ | $-\theta'(0)$ |
|---|---|---|---|---|---|
| 0 | 0.2 | 0.5 | 0.364526 | 0.055001 | 0.724584 |
| | 0.6 | | 0.364526 | 0.055001 | 1.331985 |
| | 10 | | 0.364526 | 0.055001 | 8.123117 |
| 2 | 0.2 | | 1.103997 | 0.171305 | 0.724584 |
| | 0.6 | | 0.938351 | 0.121386 | 1.331985 |
| | 10 | | 0.539472 | 0.060833 | 8.123117 |
| 10 | 0.2 | | 4.061879 | 0.636518 | 0.724584 |
| | 0.6 | | 3.233653 | 0.386928 | 1.331985 |
| | 10 | | 1.239258 | 0.084162 | 8.123117 |
| 2 | 0.62 | 0.2 | 0.906068 | 0.051156 | 1.357259 |
| | | 0.6 | 0.945865 | 0.139741 | 1.357259 |
| | | 1 | 1.006589 | 0.199215 | 1.357259 |
| | | 2 | 1.153159 | 0.243891 | 1.357259 |

Table III. Values of $f'(0)$, $G'(0)$, $-\theta'(0)$ and $-\phi'(0)$ for various values of $Q$, $R$, $\upsilon_0$ and $\gamma$ for $Gr=1$, $Pr=0.73$, $M=5$, $Gc=2$, $Sc=0.62$ and $m=0.5$.

| $\upsilon_0$ | $Q$ | $R$ | $\gamma$ | $f'(0)$ | $G'(0)$ | $-\theta'(0)$ | $-\phi'(0)$ |
|---|---|---|---|---|---|---|---|
| 0.5 | 0.2 | 1.0 | 0 | 0.97439 | 0.129214 | 0.691972 | 1.094791 |
| | | | 1 | 0.933101 | 0.120081 | 0.691972 | 1.357258 |
| | | | 2 | 0.901443 | 0.113373 | 0.691972 | 1.580046 |
| | | | 4 | 0.854794 | 0.104016 | 0.691972 | 1.952686 |
| | | 0.1 | 1 | 1.018788 | 0.154687 | 0.321199 | 1.357258 |
| | | 1 | | 0.933101 | 0.120081 | 0.691972 | 1.357258 |
| | | 5 | | 0.884563 | 0.104988 | 0.990944 | 1.357258 |
| | | 10 | | 0.87527 | 0.102452 | 1.059902 | 1.357258 |
| | −0.8 | 1 | | 0.910127 | 0.113601 | 0.888575 | 1.357258 |
| | −0.4 | | | 0.918499 | 0.115929 | 0.814637 | 1.357258 |
| | 0.0 | | | 0.927918 | 0.118595 | 0.734657 | 1.357258 |
| | 0.4 | | | 0.938653 | 0.121688 | 0.647199 | 1.357258 |
| | 0.8 | | | 0.951083 | 0.125338 | 0.550263 | 1.357258 |
| −1.0 | 0.2 | | | 0.882229 | 0.117754 | 0.400328 | 0.832471 |
| −0.5 | | | | 0.908172 | 0.121928 | 0.490024 | 0.989401 |
| 0.0 | | | | 0.92515 | 0.122601 | 0.587502 | 1.164834 |
| 0.5 | | | | 0.933101 | 0.120081 | 0.691972 | 1.357258 |
| 0.8 | | | | 0.93375 | 0.11728 | 0.757677 | 1.480146 |

the usual fact that suction stabilizes the boundary layer growth. By the imposition of wall fluid suction, the fluid in the boundary layer enters into the inside of the body through narrow slits on the wall and by doing so, the boundary layer separation can be prevented.

Figures 6–8 show the influence of the chemical reaction parameter $\gamma$ on the primary velocity, secondary velocity and concentration profiles in the boundary layer, respectively. Increasing the chemical reaction parameter produces a decrease in the species concentration. In turn, this causes

Copyright © 2009 John Wiley & Sons, Ltd.

DOI: 10.1002/fld

the concentration buoyancy effects to decrease as $\gamma$ increases. Consequently, less flow is induced along the plate resulting in decrease in the fluid primary velocity in the boundary layer. In addition, increasing the chemical reaction parameter leads to decrease in the secondary velocity profiles. These behaviors are clearly depicted in Figures 6–8.

Figures 9 and 10 display the effects of the thermal radiation parameter $R$ on the primary velocity and the temperature profiles in the boundary layer, respectively. Decreasing the thermal radiation parameter $R$ produces significant increase in the thermal state of the fluid causing its temperature to increase. This increase in the fluid temperature induces by virtue of the thermal buoyancy effect more flow in the boundary layer causing the velocity of the fluid there to increase.

Figures 11 and 12 show the effects of the heat generation or absorption parameter $Q$ and the Prandtl number $Pr$ on the primary velocity and temperature profiles, respectively. It is clear that as heat generation or absorption parameter increases, an increase in the fluid temperature occurs and through the thermal buoyancy effect, the primary velocity increases. In addition, increasing the values of the Prandtl number leads to decreases on both the primary velocity and temperature profiles.

Figures 13 and 14 present the effects of the magnetic field parameter $M$ and the Grashof number $Gr$ on the primary and secondary velocities, respectively. Application of a transverse magnetic field produces a resistive force in the $x$-direction and a motive force in the $z$-direction. This causes the primary velocity to decrease while the secondary velocity increases as the magnetic field parameter increases. In addition, increasing the Grashof number leads to increase in both velocity profiles as clearly seen in Figures 13 and 14.

Figures 15 and 16 display the effects of the Hall parameter $m$ on the profiles of the primary and secondary velocities, respectively. For the parametric conditions used to produce these figures, it is predicted that both the primary and secondary velocities increase as the Hall parameter $m$ increases.

Table I depicts the effects of some material parameters ($Gr$, $Pr$, $M$) on the skin-friction-related coefficients $f'(0)$, $G'(0)$ and the rate of heat transfer $-\theta'(0)$ for the fixed values $Gc=2$, $Q=0.2$, $Sc=0.62$, $R=1$, $\upsilon_0=0.5$, $\gamma=1$ and $m=0.5$. It is clearly observed from this table that the value of $f'(0)$ increases as the Grashof number $Gr$ increases while it decreases as either of the Prandtl number $Pr$ or the magnetic field parameter $M$ increases. However, the value of $G'(0)$ increases as either $Gr$ or $M$ increases while it decreases as $Pr$ increases. In addition, the values of the heat transfer rate increase as the Prandtl number increases while it does not change due to changes in either of the Grashof number or the magnetic field parameter. This is expected since the energy Equation (19) is uncoupled from the momentum Equations (17) and (18).

Table II illustrates the influence of the modified Grashof number $Gc$, Schmidt number $Sc$ and the Hall parameter $m$ on $f'(0)$, $G'(0)$ and the mass transfer rate $-\phi'(0)$ for the fixed values $Gr=1$, $Q=0.2$, $Pr=0.73$, $R=1$, $\upsilon_0=0.5$, $\gamma=1$ and $M=5$. It is observed that the values of $f'(0)$ and $G'(0)$ increase as the modified Grashof number $Gr$ and the Hall parameter $m$ are increases while they decrease as the Schmidt number $Sc$ increases. In addition, the value of mass transfer rate $-\phi'(0)$ increases as the Schmidt number increases while it remain unchanged as the modified Grashof number or the Hall parameter change. This also expected since the concentration species Equation (20) is uncoupled from the momentum Equations (17) and (18).

Table III illustrates the influence of the suction/injection parameter $\upsilon_0$, heat generation or absorption parameter $Q$, thermal radiation parameter $R$ and the chemical reaction parameter $\gamma$ on the skin-friction parameters $f'(0)$, $G'(0)$, heat transfer rate $-\theta'(0)$ and the mass transfer rate $-\phi'(0)$

Copyright © 2009 John Wiley & Sons, Ltd.

DOI: 10.1002/fld

for the fixed values $Gr=1$, $Pr=0.73$, $M=5$, $Gc=2$, $Sc=0.62$ and $m=0.5$. It is seen that the values of $f'(0)$ and $G'(0)$ decrease as the chemical reaction parameter $\gamma$, and the thermal radiation parameter $R$ increases, while the values of $f'(0)$ and $G'(0)$ increase as the heat generation or absorption parameter $Q$ increases. In addition, the value of $f'(0)$ increases as the suction/injection parameter $\upsilon_0$ increases while the value of $G'(0)$ increases for increased injection conditions ($\upsilon_0<0$) and decreases as the suction conditions ($\upsilon_0>0$) increase. In addition, the values of heat transfer rate $-\theta'(0)$ increase as either of the thermal radiation parameter $R$ or the suction/injection parameter $\upsilon_0$ increases while they decrease as the heat generation or absorption parameter $Q$ increases. Furthermore, the values of mass transfer rate $-\phi'(0)$ increase as either of the chemical reaction parameter $\gamma$ or the suction/injection parameter $\upsilon_0$ increases.

## 5. CONCLUSIONS

The governing equations for unsteady free convective heat and mass transfer along an infinite vertical porous plate in the presence of a transverse magnetic field, Hall current, thermal radiation, heat generation or absorption and chemical reaction were developed and transformed into similarity equations. The resulting equations were then solved numerically using a fourth-order Runge–Kutta scheme with the shooting method. Graphical results for the primary and secondary velocities, temperature and concentration profiles and tabulated values for the skin-friction coefficients and heat and mass transfer rates were presented for various values of the material parameters. The conclusions of the study were as follows:

- The velocity, temperature and concentration profiles increased for injection conditions and decreased for suction conditions.
- The behavior of primary velocity was similar with that of the secondary velocity for the effects of all material parameters except the increase of the magnetic field parameter for which the primary velocity decreased while the secondary velocity increased.
- Increasing the chemical reaction parameter produced decrease in the concentration and velocity profiles.
- The velocity and temperature profiles increased as the heat generation or absorption parameter increased or as the radiation parameter decreased.
- The velocity profiles increased as either of the Hall parameter or the Grashof number increased.
- The effects of all material parameters on the skin-friction coefficients in the $x$-direction and $z$-direction are the same except for the effect of magnetic field parameter.
- The skin-friction coefficients in the $x$-direction and $z$-direction increased as either of the heat generation or absorption parameter, the Grashof or modified Grashof numbers or the Hall parameter increased while they decreased as either of the chemical reaction parameter, the thermal radiation parameter, Prandtl number or the Schmidt number increased.
- The heat transfer rate increased as either of the thermal radiation parameter, the suction/injection parameter or the Prandtl number increased while it decrease as the heat generation or absorption parameter was increased.
- The mass transfer rate increased as either of the chemical reaction parameter, the suction/injection parameter or the Schmidt number increased.

Copyright © 2009 John Wiley & Sons, Ltd.

DOI: 10.1002/fld

## NOMENCLATURE

| | |
|---|---|
| $B_0$ | Strength of magnetic field |
| $C^*$ | Arbitrary constant |
| $C$ | Concentration |
| $C_p$ | Specific heat at constant pressure |
| $D$ | Mass diffusivity |
| $h$ | Scaling parameter |
| $f$ | Primary velocity |
| $G$ | Secondary velocity |
| $g$ | Acceleration due to gravity |
| $k$ | Thermal conductivity |
| $m_{\mathrm{w}}$ | Mass flux |
| $m$ | Hall parameter |
| $Nu$ | Nusselt number |
| $Pr$ | Prandtl number |
| $Q_0$ | Heat generation or absorption constant |
| $q_{\mathrm{w}}$ | Local wall heat flux |
| $q_{\mathrm{r}}$ | Radiative heat flux |
| $Sc$ | Schmidt number |
| $Sh$ | Sherwood number |
| $T$ | Temperature |
| $T_{\mathrm{w}}$ | Wall temperature |
| $u$ | Velocity in the $x$-direction |
| $\upsilon$ | Suction velocity |
| $\upsilon_0$ | Non-dimensional transpiration parameter |
| $w$ | Velocity in the $z$-direction |

*Greek symbols*

| | |
|---|---|
| $\beta_T$ | Coefficient of thermal expansion |
| $\beta_C$ | Coefficient of concentration expansion |
| $\gamma$ | Chemical reaction parameter |
| $\nu$ | Kinematic viscosity |
| $\phi$ | Dimensionless concentration |
| $\theta$ | Dimensionless temperature |
| $\mu_e$ | Magnetic permeability |
| $\rho$ | Density of the fluid |
| $\sigma$ | Electrical conductivity |

*Subscripts*

| | |
|---|---|
| w | Refers to wall condition |
| $\infty$ | Refers to ambient condition |

*Superscript*

| | |
|---|---|
| $'$ | Differentiation with respect to $\eta$ |

Copyright © 2009 John Wiley & Sons, Ltd.

DOI: 10.1002/fld

## REFERENCES


1. Fan JR, Shi JM, Xu XZ. Mixed convective heat and mass transfer over a horizontal moving plate. *Acta Mechanica* 1998; **126**:59–67.
2. Hossain MA, Ahmed M. Forced and free convection with uniform surface heat flux conditions. *International Journal of Heat and Mass Transfer* 1990; **33**:571–575.
3. Chamkha AJ, Khaled AR. Similarity solutions for hydromagnetic simultaneous heat and mass transfer. *Heat and Mass Transfer* 2001; **37**:117–123.
4. Vajravelu K, Nayfeh J. Hydromagnetic convection at a cone and a wedge. *International Communications in Heat and Mass Transfer* 1992; **19**:701–710.
5. Vajravelu K, Hadjinicolaou A. Heat transfer in a viscous fluid over a stretching sheet with viscous dissipation and internal heat generation. *International Communications in Heat and Mass Transfer* 1993; **20**:417–430.
6. Anjali Devi SP, Kandasamy R. Effects of chemical reaction heat and mass transfer on non-linear MHD laminar boundary-layerflow over a wedge with suction or injection. *International Communications in Heat and Mass Transfer* 2002; **29**:707–716.
7. Sieniutycz S. Nonlinear macrokinetics of heat and mass transfer and chemical or electrochemical reactions. *International Journal of Heat and Mass Transfer* 2004; **47**:515–526.
8. Singh AK, Raptis A. *Modelling Simulation and Control* (1st edn), vol. 8. B. AMSF Press, 1987.
9. Ram PC. Effects of Hall and ion-slip currents on free convective heat generating flow in a rotating fluid. *International Journal of Energy Research* 1995; **19**:371–376.
10. Seddeek MA, Aboeldahab EM. Radiation effects on unsteady MHD free convection with Hall current near an infinite vertical porous plate. *International Journal of Mathematics and Mathematical Sciences* 2001; **26**:249–255.
11. Sattar MA, Hossain MM. Unsteady hydromagnetic free convection flow with Hall current and mass transfer along an accelerated porous plate with time dependent temperature and concentration. *Canadian Journal of Physics* 1992; **70**(5):369–374.
12. Sattar MA. Free convection and mass transfer flow through a porous medium past an infinite vertical porous plate with time dependent temperature and concentration. *Indian Journal of Pure and Applied Mathematics* 1994; **25**(7):759–766.
13. Alam MM, Sattar MA. Unsteady MHD free convection and mass transfer flow in a rotating system with Hall current, viscous dissipation and joule heating. *International Journal of Heat and Mass Transfer* 2000; **22**:31–39.
14. Maleque MA, Alam MS. Magnetohydrodynamic free convection and mass transfer flow past a vertical porous flat plate with Dufour and Soret effects. *Journal of Naval Architecture and Marine Engineering* 2004; **1**(1):18–25.
15. Alam MS, Rahman MM, Maleque MA. Local similarity solutions for unsteady MHD free convection and mass transfer flow past an impulsively started vertical porous plate with Dufour and Soret effects. *Thammasat International Journal of Science and Technology* 2005; **10**(3):1–8.
16. Rahman MM, Sattar MA. Transient convective flow of micropolar fluid past a continuously moving vertical porous plate in the presence of radiation. *International Journal of Applied Mechanics and Engineering* 2007; **12**(2):497–513.
17. Sparrow EM, Cess RD. *Radiation Heat Transfer*, Augment Edition. Hemisphere: Washington, DC, 1962.
18. Schlichting H. *Boundary Layer Theory*. McGraw-Hill: New York, 1968.


Copyright © 2009 John Wiley & Sons, Ltd.

DOI: 10.1002/fld